Aerosol and Air Quality Research, 18: 3147–3164, 2018

ISSN: 1680-8584 print / 2071-1409 online
doi: 10.4209/aaqr.2018.02.0064

Assessment of Adsorptive Filter for Removal of Formaldehyde from Indoor Air

Angus Shiue[1+], Shih-Cheng Hu[1+], Chao-Heng Tseng[2*], Cheng-Mao Chuang[2], Graham Leggett[3]

[1] *Department of Energy and Refrigerating Air-conditioning Engineering, National Taipei University of Technology, Taipei 10608, Taiwan*
[2] *Institute of Environment Engineering and Management, National Taipei University of Technology, Taipei 10608, Taiwan*
[3] *MIRICO Ltd., OX11 0QX, United Kingdom*

ABSTRACT

We varied face velocities and initial formaldehyde concentrations to investigate the formaldehyde removal performance of coconut shell activated carbon (AC) adsorptive filter media. AC surface were rather uneven, with coarse and small pores, and with amorphously formed irregular layer structures. C, O, Mg, P etc. were detected, which showed the existence of MgO in AC. The AC surface area was 1333.3304 m^2 g^{-1}, and ketone -C=O bonds were successfully grafted onto the carbon. At any given face velocity, the experimental results indicate that the adsorption capacity increased and the breakthrough time decreased as the initial concentration increased. The breakthrough behavior of the AC adsorptive filter could henceforth be evaluated with confidence using the breakthrough curves predicted by the Yoon-Nelson model. Of the three kinetic models that were assessed, the experimental and calculated results show that the correlation coefficient and mean absolute performance error (MAPE) of the pseudo-second-order model generated the best approximation of the kinetic dynamics of the adsorption process—better than those of the pseudo-first-order model and intraparticle diffusion model. Both the intraparticle diffusion model and the membrane diffusion affected the overall rate of the adsorption process by more than one step. The equilibrium data of the AC adsorptive filter media was found to best fit the Langmuir model. The D-R equation predicted the equilibrium capacity of AC at a relative pressure of 0.151.

Keywords: Adsorption; Breakthrough; Kinetic model; Formaldehyde.

INTRODUCTION

Human beings typically spend more than 90% of their waking hours in indoor environments. As such, pollutants found in indoor air may in many cases represent a higher hazard to human health than those present in the outdoor environment (Brunsgaard *et al.*, 2012). Recent changes to building regulations have demanded much higher air-tightness requirements for residential and commercial buildings for reasons of improved energy conservation. As a result, there exists the potential for increased concentrations of volatile organic compounds (VOCs) within indoor environments. The negative impact on health and well-being and comfort (Chuck and Kim, 2013) of occupants in air-tight housing is well documented. Among VOCs, formaldehyde (HCHO) has long been established as a hazardous and harmful substance (Mui *et al.*, 2008). The primary source of formaldehyde found as a pollutant in indoor air is pressed wood products manufactured using urea formaldehyde resins (U.S. Consumer Product Safety Commission, 2015).

There are several studies on air cleaning technologies for indoor formaldehyde removal. UV photolysis is limited due to its trend to produce ozone and radicals with harmful effects. Photocatalytic oxidation has been utilized for ppm levels of contaminant degradation and ppbv concentrations need to be measured, and their main deficiencies are the short lifetime of the catalyst and the creation of harmful by-products. Cold or non-thermal plasma are not yet on the market (Luengas *et al.*, 2015). These major technical issues also have limitations like high energy consumption and low removal efficiency (Gilbert *et al.*, 2008; Mo *et al.*, 2008). Biological degradation (Lu *et al.*, 2012) and botanical air filtration are still under development, currently operating at low efficiency and with insufficient understanding of long-term safety (Wang *et al.*, 2014; Luengas *et al.*, 2015). At this time, neither of these techniques is broadly employed for indoor pollutant removal (Lu *et al.*, 2012). Activated carbon adsorption is a simple, effective, and low cost method to reduce the concentrations of formaldehyde removal in indoor air (Lu *et al.*, 2015).

[+] These authors contributed equally to this work.

[*] Corresponding author.
Tel.: +886-2-27712171 ext. 4141
E-mail address: tsengco@ntut.edu.tw

The primary purpose of this study characterized the physical and chemical properties of the AC by Scanning electron microscope (SEM), X-ray diffraction (XRD), Energy Dispersive X-ray Spectroscopy (EDS), Brunauer-Emmett-Teller (BET), and Fourier transform infrared spectroscopy (FTIR) analysis to investigate the equilibrium, breakthrough behavior, and the applicable assessment of three kinetic models: pseudo-first-order, pseudo-second-order and intraparticle diffusion. The latter assessment was conducted under various experimental conditions using the correlation coefficient (R^2) and the mean absolute percentage error (MAPE) to characterize the kinetic data. As a result, this study provided the essential parameters to consider when designing and operating an adsorptive purifier for removal of formaldehyde from indoor air, and implementing strategies to improve air quality in the indoor environment.

MATERIALS AND METHODS

Principle

Adsorptive Capacity

This study used the testing method of VanOsdell *et al.* (1996) shown in Fig. 1. The mixed air passes through the adsorbent. Removal efficiency (η) was calculated with the initial concentration (C_0). Adsorption capacity (q_t) is defined as follow (Shiue *et al.* 2010):

$$q_t = C_0 V \int \eta(t)dt \times \frac{1}{0.082} \times \frac{1}{273+k} \times M \times 10^{-6} \quad (1)$$

Breakthrough

Generally, it is not practicable to measure activated carbon filter breakthrough time against formaldehyde concentration in real indoor environments. When the outlet concentration reached 2% of the initial concentration, the breakthrough time was determined (Dehdashti *et al.*, 2011). While changing only formaldehyde concentration, simplified breakthrough time estimation is shown as (Cheng and Tsai, 2007; Cheng, 2008; Shiue *et al.*, 2010):

$$\frac{t_{b,1}}{t_{b,2}} = \left(\frac{C_{0,1}}{C_{0,2}} \right)^a \quad (2)$$

where t_b is the breakthrough time, C_0 is the initial (inlet) concentration of adsorbate (ppmv), α is the constant. Eq. (2) predicted the performance of the activated carbon filter.

Yoon and Nelson (1984) initially developed a simple model that proposed the rate of decrease in the probability of adsorption for each adsorbate molecule is proportional to the probability of adsorption of an adsorbate (P_{ads}) and the probability of breakthrough of the adsorbate ($1 - P_{ads}$):

$$\frac{-dP_{ads}}{dt} = k' P_{ads}(1 - P_{ads}) \quad (3)$$

Integrating Eq. (3), and defining τ as the time required for 50% breakthrough (i.e., P_{ads} = 0.5, hereinafter referred to as the stoichiometric breakthrough time):

$$t_b = \tau + \frac{1}{k'} \ln \frac{C_t}{C_0 - C_t} \quad (4)$$

where k' is a rate constant, C_t is the breakthrough (effluent) concentration of adsorbate. The calculation of theoretical breakthrough curves for a single-component system requires the determination of the parameters k' and t for the adsorbate of interest.

In accordance with Eq. (4), the value of k' can be got from the slope of the plot $\ln[C_t/(C_0 - C_t)]$ versus breakthrough time t, and the value of t (50% breakthrough time) can be decided as the time at Q = 0.5 (i.e., $C_t = C_0/2$). Applying k' and t of Eq. (4), one may cause the complete breakthrough curve for a given set of experimental conditions. Furthermore, Yoon and Nelson (1984) have proposed the following equation:

$$K = k't \quad (5)$$

where K is a proportionality constant for a given adsorbate and determined type of adsorbent. Both k' and t alternatively rely on the concentration of the adsorbate and the face velocity.

Kinetic Model

The pseudo-first-order equation is expressed by Lagergren equation (1898) as follows:

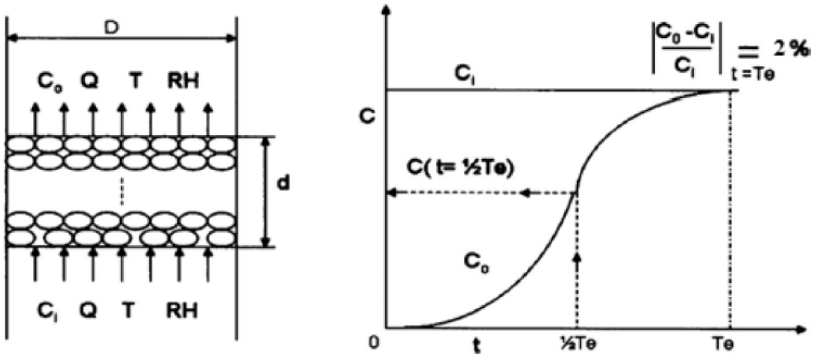

Fig. 1. Schematic diagram of testing theory.

$$\log(q_e - q_t) = \log q_e - \frac{k_1}{2.303}t \quad (6)$$

where q_e is the amount of adsorbed formaldehyde per unit weight of adsorbent, q_t is the amount of adsorbate adsorbed at time t.

The pseudo-second-order model is shown as (Ho and McKay, 1999):

$$\frac{t}{q_t} = \frac{1}{k_2 q_e^{\,2}} + \frac{1}{q_e}t \quad (7)$$

The intraparticle diffusion model is described as follows (Guibal, 1998):

$$q_t = k_i t^{1/2} + C \quad (8)$$

Error Analysis

Mandal *et al.* (2015) used correlation coefficient (R^2) and mean absolute performance error (MAPE) values to verify the experimental data for the most suitable kinetic model. These expected indices were computed by utilizing the following equations:

$$R^2 = \frac{\left[\sum_{i=1}^{n}\left(q_{pre} - \bar{q}_{pre}\right)\left(q_{\exp} - \bar{q}_{\exp}\right)\right]^2}{\sum_{i=1}^{n}\left(q_{pre} - \bar{q}_{pre}\right)^2 \sum_{i=1}^{n}\left(q_{\exp} - \bar{q}_{\exp}\right)^2} \quad (9)$$

$$MAPE = \frac{1}{n}\sum_{i=1}^{n}\left|\frac{q_{\exp} - q_{pre}}{q_{\exp}}\right| \times 100 \quad (10)$$

where q_{pre} and q_{exp} are the expected and measured values of formaldehyde concentration, respectively; $\bar{q}$ illustrates the average values of related q; n is the total number of observations.

Adsorption Isotherm Model

Between adsorbed and free formaldehyde in air, the equilibrium is given by the linearized Langmuir isotherm model as per the following equation (Cheng and Tsai, 2007; Bernabe *et al.*, 2015):

$$\frac{C_e}{q_e} = \frac{1}{q_{\max} K_L} + \left(\frac{1}{q_{\max}}\right) C_e \quad (11)$$

where q_e is the adsorbed amount of formaldehyde per unit weight of adsorbent at equilibrium; C_e is concentration of free formaldehyde in air; $q_{\max}$ is maximum adsorption capacity; and K_L is the Langmuir's adsorption equilibrium constant related to the affinity of the binding sites; this phenomenon has been described before (Cheng and Tsai, 2007; Bernabe *et al.*, 2015).

Linearizing the Freundlich isotherm model is shown as (Cheng and Tsai, 2007; Bernabe *et al.*, 2015):

$$\log q_e = \log k_f + 1/n \log C_0 \quad (12)$$

where k_F and n are Freundlich constants, which related to the adsorption intensity and adsorption capacity, respectively (Cheng and Tsai, 2007; Bernabe *et al.*, 2015).

The Dubinin-Radushkevich (D-R) equation, which was initially formulated from the Polanyi adsorption potential theory and represents molecular adsorption as a pore-filling phenomenon rather than a layer-covering one, has been used to correct the Freundlich isotherms (Yao *et al.*, 2009). In accordance with the D-R equation the adsorption capacity (W), expressed as the adsorbed liquid volume per unit mass of adsorbent, is related to the adsorption potential (A) as given by (Dubinin, 1966):

$$\ln(W/W_0) = -kA^2 \quad (13)$$

and

$$A = RT\ln(P_0/P) \quad (14)$$

where W is the volumetric adsorption capacity, W_0 is the maximum adsorption space, k is the parameter for each system of adsorbate and adsorbent, A is adsorption potential, R is the universal gas constant, T is the absolute temperature, P_0 is the saturated vapor pressure at temperature T, and P is the partial pressure of the adsorbate. Combined Eqs. (13) and (14), the gas-phase partial pressure related to the adsorption capacity as follows:

$$\ln W = \ln W_0 - k[RT(P/P_0)]^2 \quad (15)$$

Experimental Methods

The 2.2 mm thickness AC-loaded nonwoven fabric filter media (provided by AIRREX Co. Ltd.) was placed into a 10 cm × 10 cm testing rig located in a temperature of 28 ± 1°C by ambient air-conditioning system. The testing airflow was controlled at relative humidity (RH) of 40 ± 2% by adjusted primary split airflow. The characteristics of fabric filter media and schematic test system diagram are shown in Table 1 and Fig. 2, respectively.

The face velocity of filter media was rated at 0.25, 0.5, and 0.75 m s^{-1} (VT110-VT115 Hotwire Thermo-anemometer). A source of compressed air was first passed through a drier, adsorbent, and high efficiency particulate air (HEPA) filter to generate a "zero air." This zero air was then blended with formaldehyde via a gas-generator to produce the challenge gas entering the test rig (Fig. 1). 99.9% grade formaldehyde solvent was filled into the gas-generator and submerged in a water bath (temperature adjustable from 15°C to 25°C). The formaldehyde entered upstream of the testing rig, controlled by passing air through a mass flow controller (Fujikin T1000). Formaldehyde concentration was fixed at 0.25, 0.56 and 0.79 ppm with ±2% deviation. A real-time formaldehyde analyzer (Formaldemeter htv-m) monitored the concentration of the challenge gas.

Characterization

Scanning electron microscope (SEM, ZEISS ΣIGMA

Table 1. Characteristics of fabric filter media (Shiue *et al*., 2010).

Raw material	Coconut shell
BET surface area ($m^2 g^{-1}$)	1145
Ash content (on dry basis) (%)	3%
Moisture content (%)	20–25%
pHzpc	6
Particle size, mesh	12 × 20 mesh
Thickness, e (mm)	2.2 mm
Weight per surface, W ($g m^{-2}$)	702.8
Specific surface area, SBET ($m^2 g^{-1}$)	931.2
Pore volume, Vp ($cm^3 g^{-1}$)	0.6762
Microporous volume, Vμp ($cm^3 g^{-1}$)	0.3264
Microporous volume percentage, %Vμp (%)	0.48%
Median micropore diameter, dμp	52.08 Å

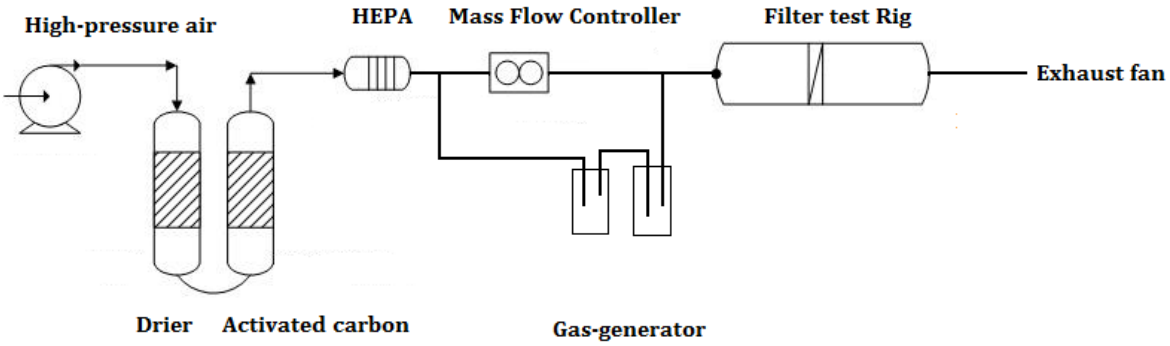

Fig. 2. Schematic diagram of the experimental system setup.

Essential) was used to study the surface morphology of the adsorbent. X-ray diffraction (XRD) is for chemical characteristics and surface morphology of adsorbent study. Energy-dispersive X-ray spectrometry (EDS, ZEISS ΣIGMA Essential) was employed for the elemental analysis of the sample. To obtain an infrared spectrum of absorption or emission of adsorbent, Brunauer-Emmett-Teller (BET, Micrometrics ASAP2020) method was used to study the surface area. Fourier-transform infrared spectra (FTIR, Spectrum one) was applied.

RESULTS AND DISCUSSION

Characterization

Scanning Electron Microscope

Fig. 3 shows the SEM image of AC under different magnification (100, 400, and 2000) magnification. Fig. 3(a) indicated the surface is smooth and distributed with small pores. Moreover, it can observe a little crack and tiny particle near the pore. From Figs. 3(b) and 3(c) the surface of AC is rather uneven, coarse and porous. The shape is columnar and lamellar on the surface because the coconuts have the cellulose sintering at high temperature.

X-Ray Diffraction (XRD)

Fig. 4 indicated XRD pattern of AC. The graph was observed that AC is amorphous. The two broad Bragg or diffraction peaks were shown around 22° and 43° indicated that the crystallites were produced by two or more of these plates layer being stacked one above the other. Irregular layer structure were formed the amorphous that the XRD diffraction peaks were broad.

Energy Dispersive X-Ray Spectroscopy (EDS)

Fig. 5 illustrated the EDS detection area of AC; element such as C, O, Mg, P etc. can be found in the AC. AC is composed of C, O, and P accounting for 77.48%, 18.71%, 3.28% respectively. And we can calculate the O/C ratio = 24.14% which means around 1.0 unit carbons are given by 24.14 unit oxygen. Some metal element like Mg with weight percentage 0.28%. Mg and P are detected in the elemental analysis of AC. The EDS analysis showed that the Mg/C ratio = 0.68%, which further proves the existence of MgO in the coconut's activated carbons.

Surface Area and Pore Size

The BET analysis showed that the surface area was 1333.3304 $m^2 g^{-1}$ after BET analysis. The identified data showed that micropore volume of AC is 0.13 $cm^3 g^{-1}$, meso volume is 0.45 $cm^3 g^{-1}$, total volume is 0.840442 $cm^3 g^{-1}$; BJH adsorption average pore diameter is 2.21361 nm in the range of 2.0–3.0 nm. The most important thing is the area between adsorption linear and desorption linear in Fig. 6.

Fourier-Transform Infrared Spectra

Fig. 7 shows FTIR spectroscopy in analysis of the functional groups. AC depended upon the experiments with molecular organic compounds that we can list the orders of

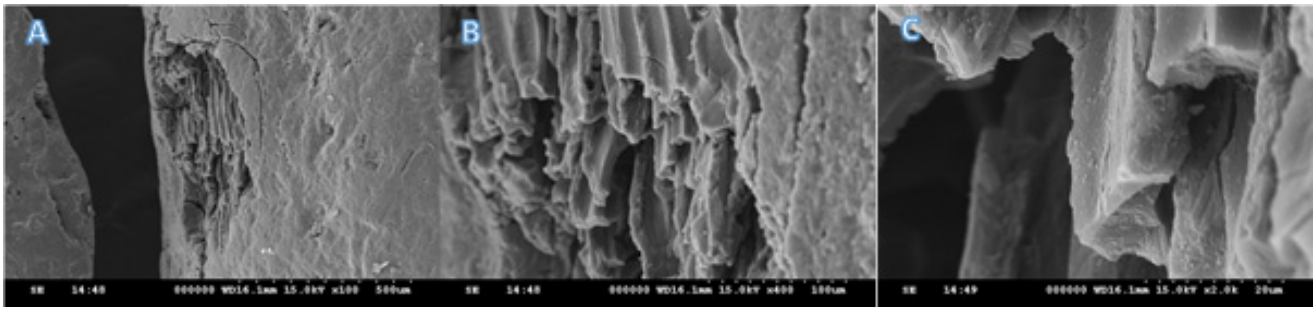

Fig. 3. SEM photographs of AC at (a) 100, (b) 400, and (c) 2,000 magnifications.

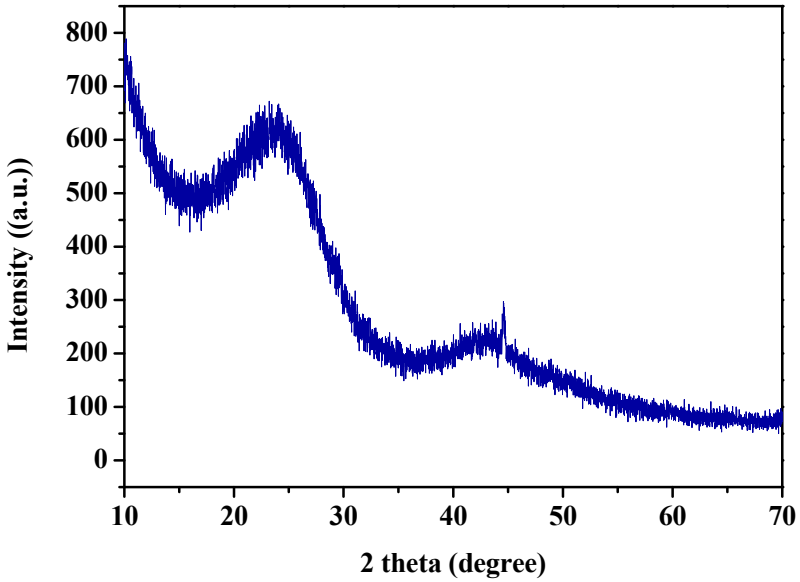

Fig. 4. XRD imagine of AC.

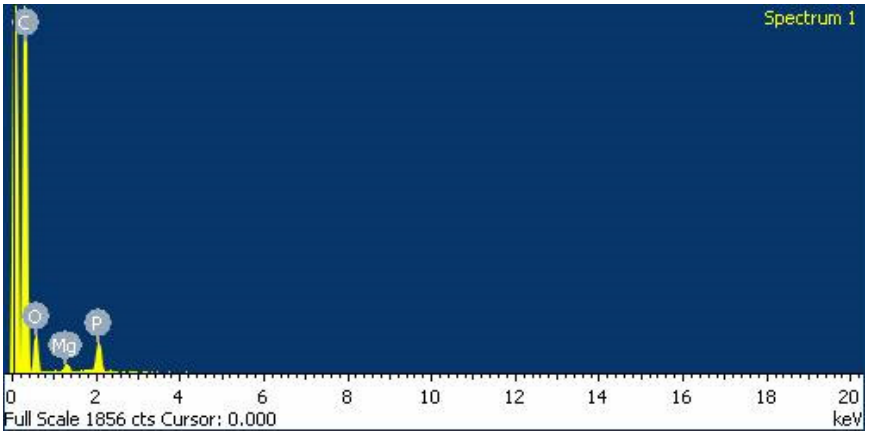

Element	Weight%	Atomic%
C	77.48	83.26
O	18.71	15.09
Mg	0.53	0.28
P	3.28	1.36
Tatals	100.00	

Fig. 5. EDS of AC.

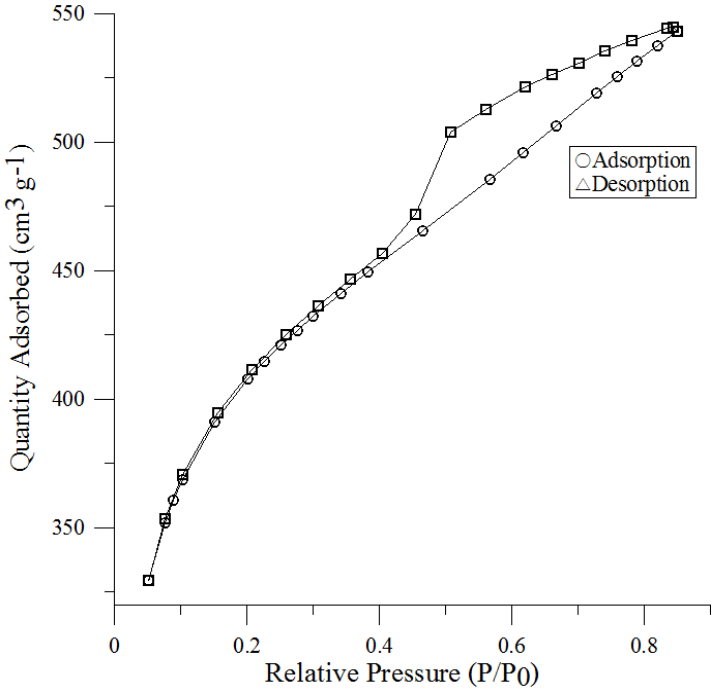

Fig. 6. Adsorption isotherms of N_2 at 77 K on AC.

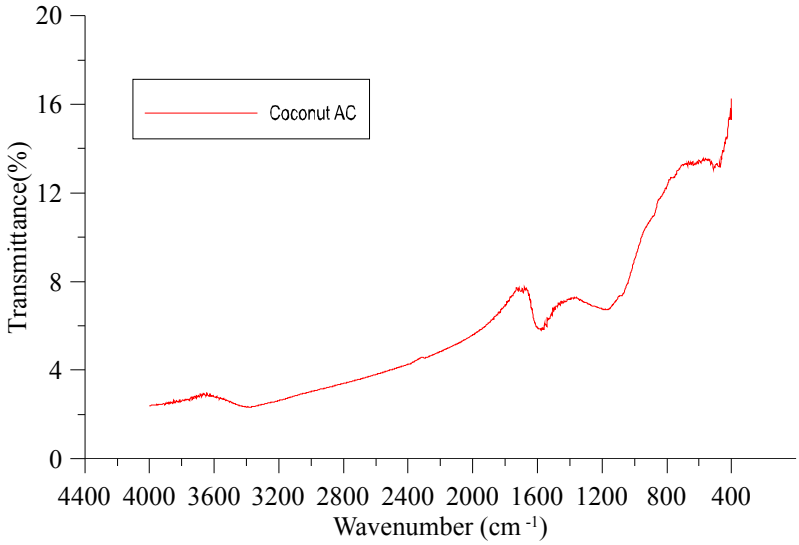

Fig. 7. FTIR imagine of AC.

the absorptive bands. It showed an intensive band 3417 cm^{-1} has been explained by stretching of ketone -C=O bonds. A weak strength bonding at 2329 cm^{-1} indicated the formation of O-H bonds from carboxylic acid (Boehm, 2002). Near 1166 and 1086 cm^{-1} has been explained by reverse stretching vibrations of carboxylic acids C-O bonds.

Adsorption Capacity

Fig. 8 presents variations in formaldehyde adsorption capacity with different inlet concentrations at different face velocities. Equilibrium time (t_t) is defined as the time when the outlet concentration is 98% of the inlet concentration. The proportional relationship between natural logarithm of equilibrium time and formaldehyde adsorption capacity (Q) is presented as the formula (Scahill *et al.*, 2004) in Table 2. These results are in agreement with Shiue *et al.* (2010) (flow rate of 0.076–0.152 m s^{-1} at an inlet toluene concentration of 10–70 ppm). As shown in Fig. 8, if the inlet concentration of the adsorbate is increased, resulting in increased velocity of diffusion into the pores of AC, adsorption may reach equilibrium faster; the equilibrium time decreased from 86 to 30 min, 64 to 24 min and 46 to 12 min, while adsorption capacity increased from 0.265 to 0.2991 mg g $media^{-1}$, 0.3244 to 0.4726 mg g^{-1}, and 0.4726 to 0.6019 mg g^{-1} at 0.25, 0.5 and 0.75 m s^{-1} face velocities, respectively.

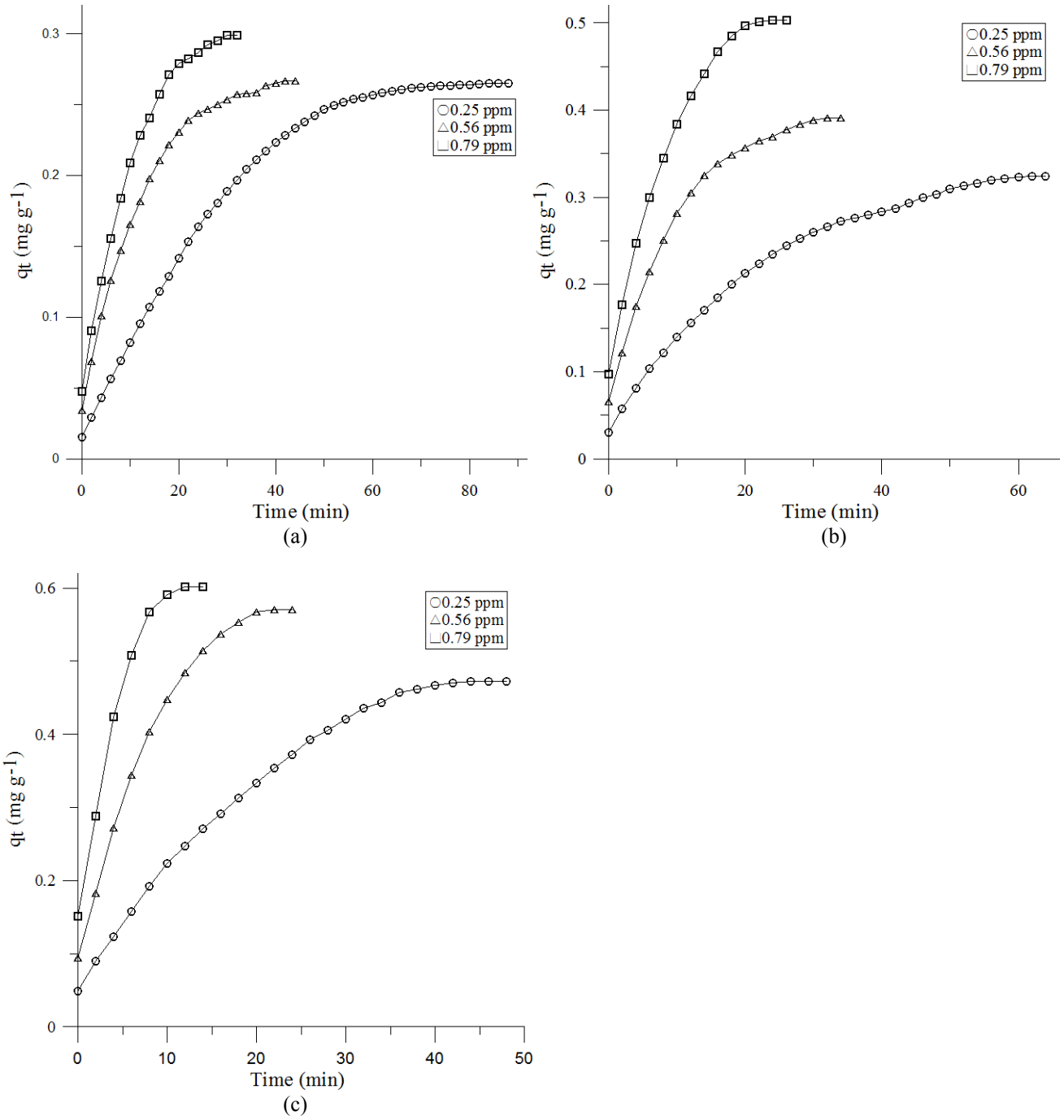

Fig. 8. Effect of concentration on formaldehyde adsorption capacity (a) 0.25 m s^{-1}, (b) 0.5 m s^{-1}, and (c) 0.75 m s^{-1}.

Table 2. Correlations of formaldehyde adsorption capacity with time and concentrations.

Face velocity (m s^{-1})	C_i (ppm)	Adsorption capacity (Q) vs. time (t)	Adsorption capacity (mg g^{-1})	t (min)
0.25	0.25	$Q = 0.081 \ln(t) - 0.0807$, $R^2 = 0.9596$	0.2650	76
	0.56	$Q = 0.0707 \ln(t) - 0.0098$, $R^2 = 0.9849$	0.2669	41
	0.79	$Q = 0.0836 \ln(t) - 0.0188$, $R^2 = 0.9861$	0.2989	33
0.5	0.25	$Q = 0.0902 \ln(t) - 0.005$, $R^2 = 0.9785$	0.3244	68
	0.56	$Q = 0.1022 \ln(t) - 0.0441$, $R^2 = 0.9904$	0.3906	38
	0.79	$Q = 0.1405 \ln(t) - 0.0638$, $R^2 = 0.9873$	0.5029	28
0.75	0.25	$Q = 0.1441 \ln(t) - 0.0815$, $R^2 = 0.9636$	0.4724	44
	0.56	$Q = 0.1695 \ln(t) - 0.0541$, $R^2 = 0.9905$	0.5701	19
	0.79	$Q = 0.1693 \ln(t) + 0.1882$, $R^2 = 0.9682$	0.6015	12

Breakthrough

Complete breakthrough is specified as the point at which the measured formaldehyde concentration at the outlet equaled its inlet concentration. Breakthrough was executed by varying initial formaldehyde concentrations from 0.25 to 0.79 ppmv at 0.25 to 0.75 m s^{-1} face velocity shown in Fig. 9. The breakthrough time was decreased from 78, 68, and 44 to 34, 28, and 14 min for 0.25 to 0.79 ppmv formaldehyde initial concentrations at 0.25 to 0.75 m s^{-1} face velocity, respectively. This phenomenon has been described before (Cheng and Tsai, 2007, Jo and Chun, 2014). Additionally, the breakthrough behavior also was decreased from 78, 68, and 34 to 44, 28, and 14 min for 0.25 to 0.75 m s^{-1} face velocity at formaldehyde initial concentration of 0.25, 0.56 and 0.79 ppmv, respectively.

The relationships between various logarithmic formaldehyde initial concentrations and various logarithmic breakthrough times are expressed in Fig. 10 and Table 3. The slopes of the lines were smaller for the formaldehyde with lower face velocity at the same concentration.

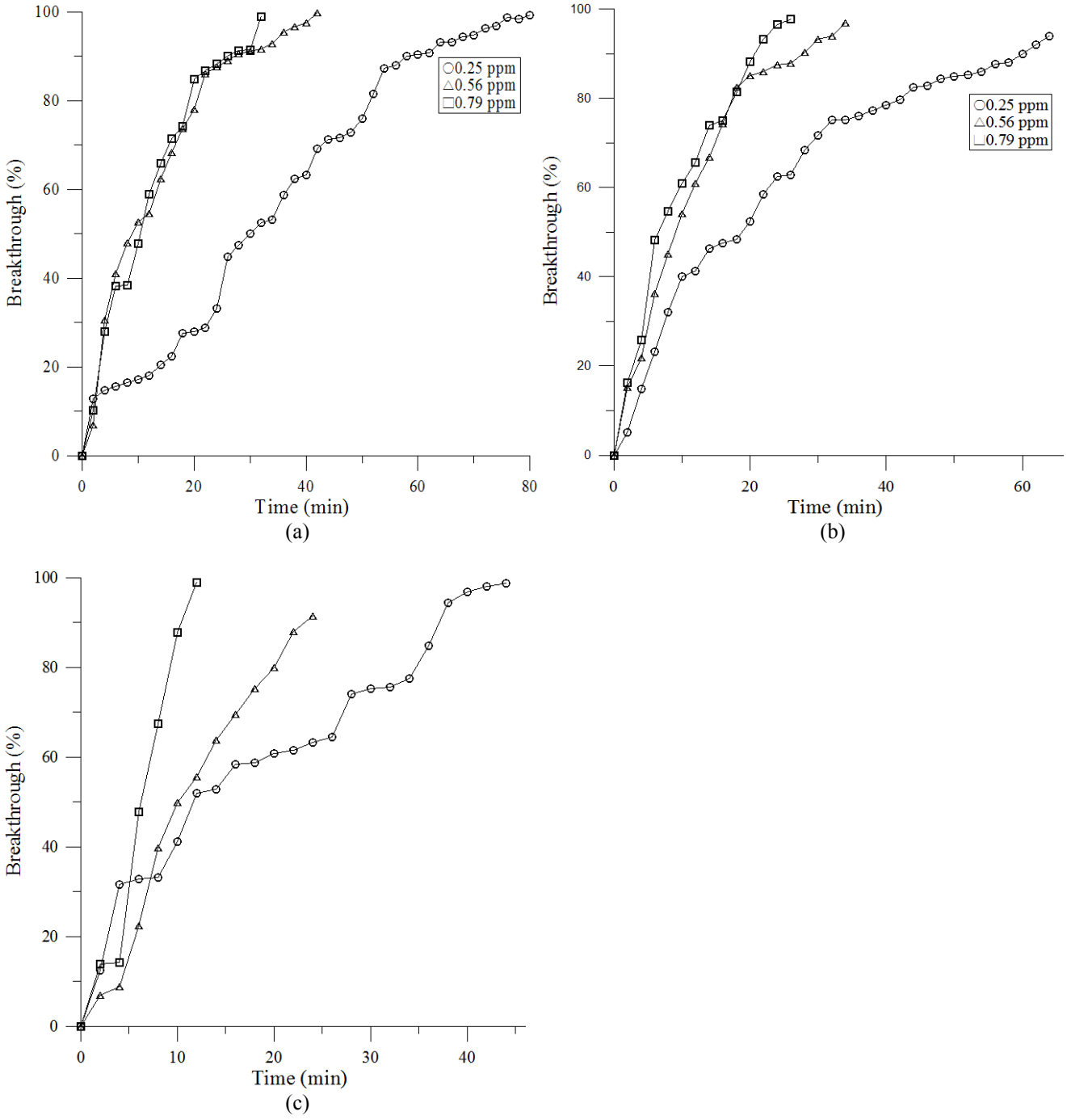

Fig. 9. The breakthrough curves of formaldehyde adsorption at various concentration and various face velocity (a) 0.25 m s^{-1}, (b) 0.5 m s^{-1}, and (c) 0.75 m s^{-1}.

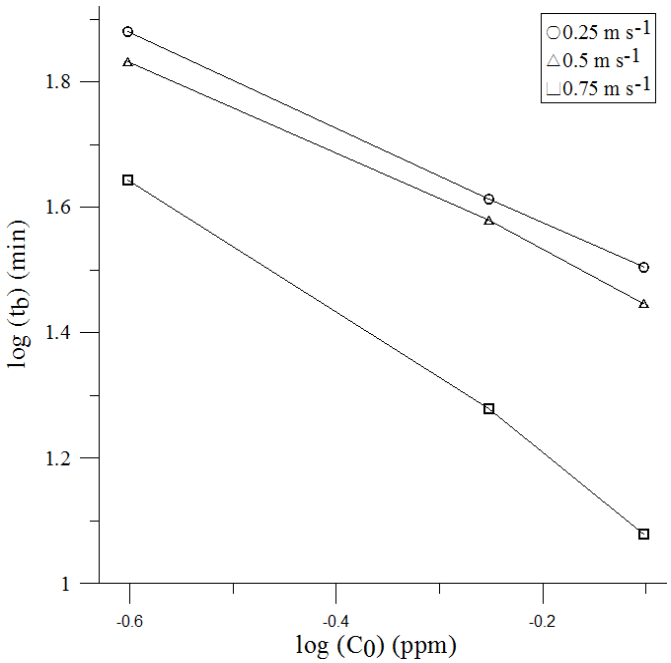

Fig. 10. The relationships between formaldehyde concentrations and breakthrough times.

Table 3. The relationships between formaldehyde concentrations and breakthrough times.

Face velocity (m s^{-1})	Breakthrough time vs. Initial concentration
0.25	$t_b C_0^{0.1761} = 26.662$, $R^2 = 0.9998$
0.5	$t_b C_0^{0.1729} = 23.812$, $R^2 = 0.9975$
0.75	$t_b C_0^{0.077} = 9.526$, $R^2 = 0.9963$

The plots of Eq. (4) at various face velocities (Fig. 11) yielded linear curves with excellent correlations, the end-point of the regression analyses used 50% breakthrough, i.e., $\ln(c_b/c_i - c_b = 0)$. Table 4 listed the values of the slopes (k') and the intercept of ($-k$). Both k' and τ are dependent on the adsorbate inlet concentration. The rate constant k' increased with increasing formaldehyde inlet concentration, as the stoichiometric breakthrough time τ decreased. Also, both k' and τ were significantly affected by the face velocity; i.e., the value of k' increased with increasing face velocity, while the value of τ decreased. Due to k' and τ act in reverse trend, one would predict that k would be a constant with a well-behaved breakthrough times presented in Fig. 11. Certainly, as interpreted in Table 4, the value of proportionality constant K (2.60 ± 0.47) could be utilized as a basis of prevision for other hypothetical formaldehyde concentrations and face velocities.

Adsorption Kinetic Models

To determine the sorption mechanism, three common kinetic models, pseudo-first-order, pseudo-second-order, and intra-particle diffusion models, were applied to empirically analyze kinetic sorption data.

Pseudo-first-order Model

The plot of pseudo-first-order kinetics is shown in Fig. 12. Table 5 summarized the calculated constants according to the pseudo-first-order equation along with correlation coefficients (r_1^2). The adsorption amount $q_{e,1}$ of formaldehyde increased from 0.264, 0.324, and 0.472 to 0.298, 0.502, and 0.601 mg g^{-1} for 0.25 to 0.79 ppmv formaldehyde initial concentrations at 0.25 to 0.75 m s^{-1} face velocity, respectively. It shows formaldehyde removal efficiency is dependent on initial concentration. In addition, the amount of formaldehyde adsorption decreased from 0.571, 0.787, and 0.986 to 0.291, 0.441, and 0.820 mg g $media^{-1}$ for 0.25 to 0.75 m s^{-1} face velocity at 0.25, 0.56 and 0.79 ppmv formaldehyde initial concentration, respectively. The removal efficiency of formaldehyde is also dependent on face velocity. Moreover, the calculated data of $q_{e,1}$ are closer to the experimental data. With the initial concentration increased from 0.25 to 0.79 ppm at face velocity 0.25 to 0.75 m s^{-1}, the rate constant (k_1) values were increased from 0.77 to 0.145, 0.082 to 0.227 and 0.125 to 0.547 min^{-1}, respectively. The rate constant (k_1) of the pseudo-first-order rate model is linearly related to formaldehyde initial concentration (C_0) is shown in Fig. 13. This result is similar to the findings of many previous studies (Saeid and Bahare, 2006).

Pseudo-second-order Model

Fig. 14 presents a plot of the pseudo-second-order kinetics for the formaldehyde adsorption onto AC filter media. Table 5 summarizes the calculated constants (k_2) of the pseudo-second-order equation along with correlation coefficients (r_2^2). The adsorption amount ($q_{e,2}$) of the

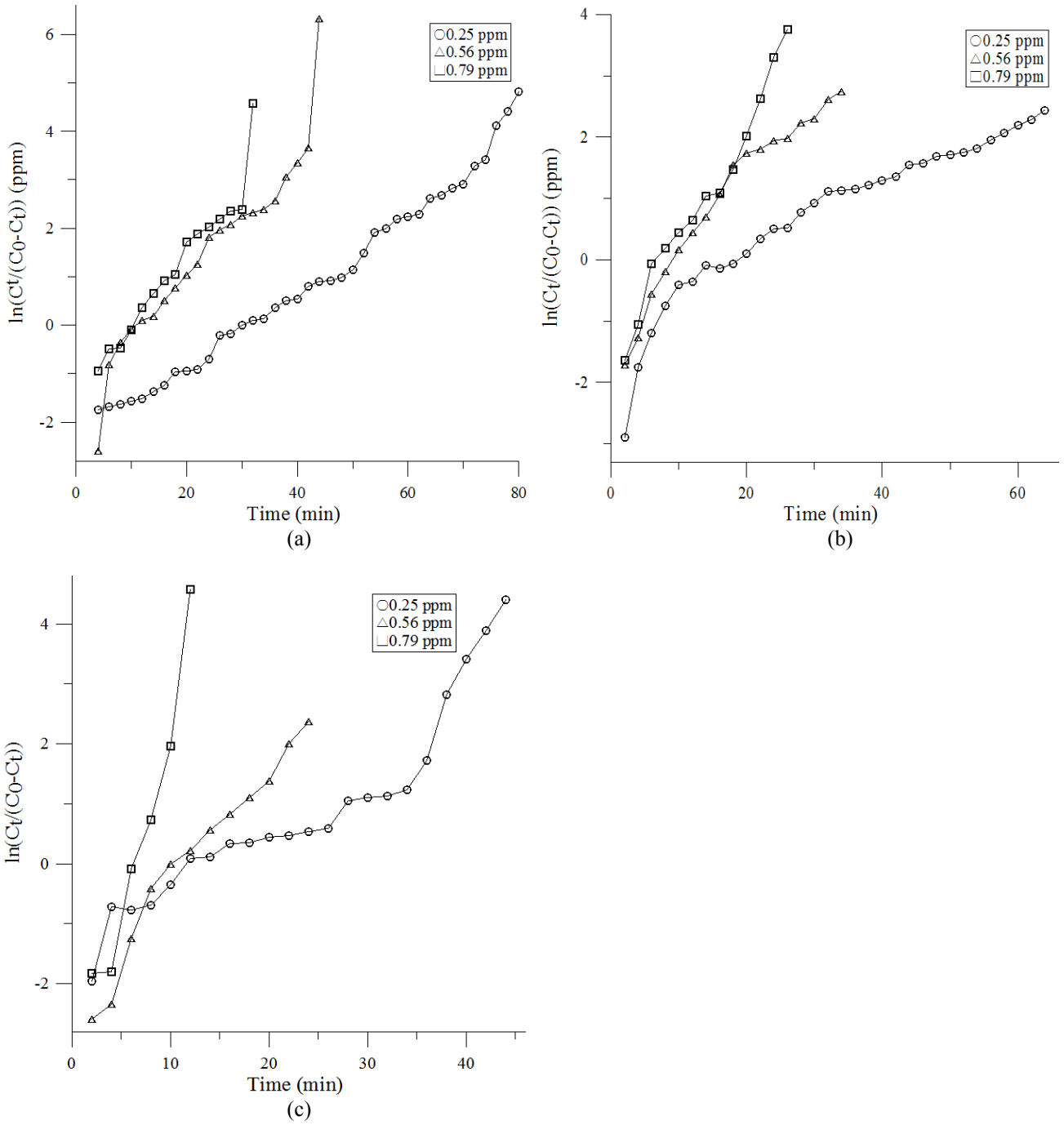

Fig. 11. Effect of concentration on $\ln[(C_i - C_b)/C_b]$ (a) 0.25 m s^{-1}, (b) 0.5 m s^{-1}, and (c) 0.75 m s^{-1}.

Table 4. The theoretical parameters *k*', *t*, and *K*.

Face velocity (m s^{-1})	Concentration (ppm)	*k*' (min^{-1})	*t* (min)	*K*	R^2
0.25	0.25	0.081	40	3.232	0.981
	0.56	0.124	22	2.737	0.978
	0.79	0.143	16	2.294	0.972
0.5	0.25	0.056	32	1.792	0.973
	0.56	0.183	17	3.114	0.972
	0.79	0.201	13	2.613	0.972
0.75	0.25	0.086	22	1.892	0.973
	0.56	0.197	12	2.359	0.979
	0.79	0.565	6	3.389	0.972

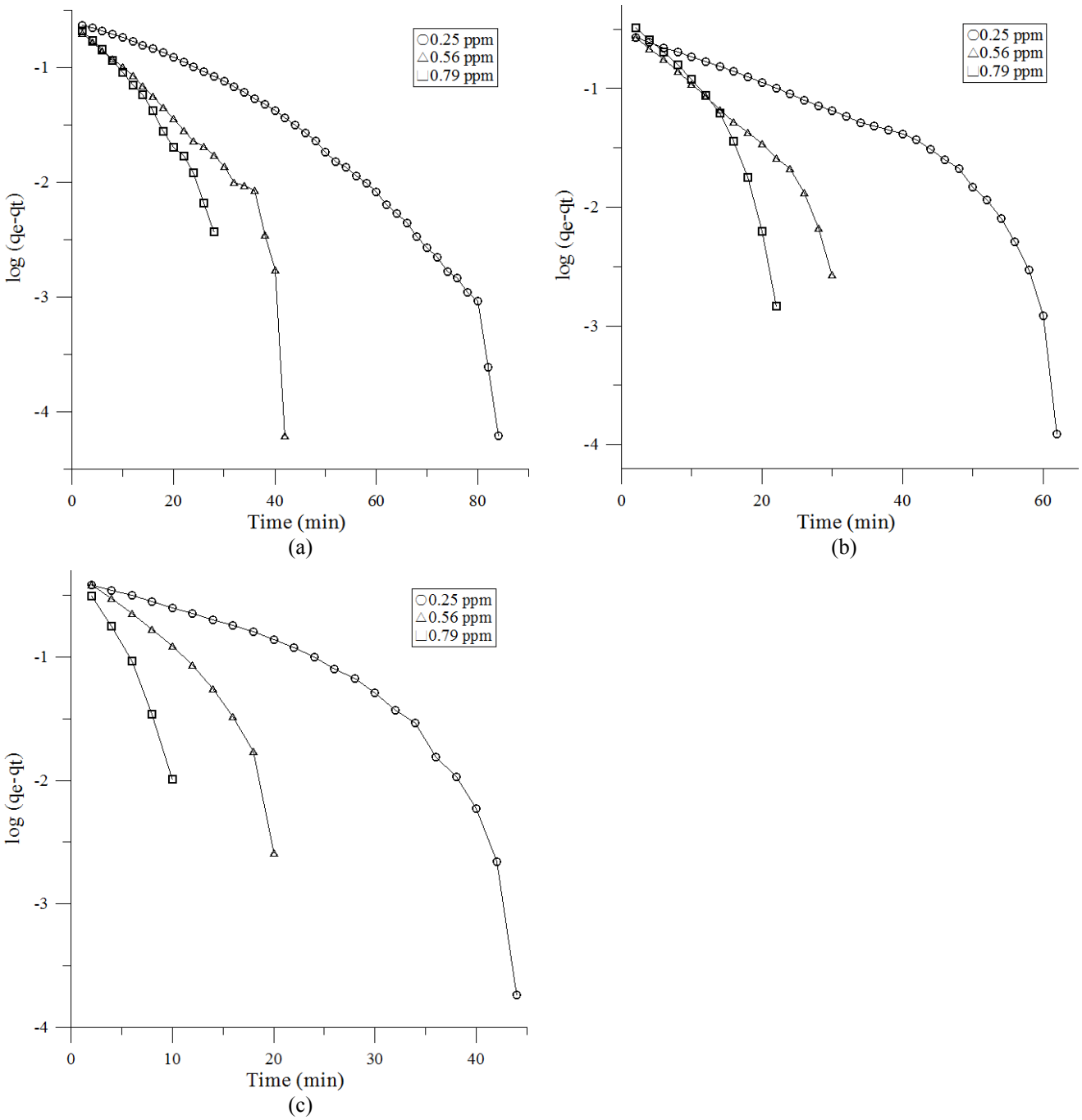

Fig. 12. Plot of Pseudo-first order kinetics at face velocity (a) 0.25 m s^{-1}, (b) 0.5 m s^{-1}, and (c) 0.75 m s^{-1}.

formaldehyde increased from 0.309, 0.329, and 0.715 to 0.498, 0.785, and 0.721 mg g^{-1} $media^{-1}$ for 0.25 to 0.79 ppmv formaldehyde initial concentrations at 0.25 to 0.75 m s^{-1} face velocity, respectively. The formaldehyde removal is based on initial concentration. In addition, the amount of formaldehyde adsorption $q_{e,2}$ increased from 0.309, 0.402, and 0.498 to 0.35, 0.522, and 0.919 mg g^{-1} $media^{-1}$ for 0.25 to 0.75 m s^{-1} face velocity at 0.25, 0.56 and 0.79 ppmv formaldehyde initial concentration, respectively. It shows that the formaldehyde removal efficiency is also dependent on face velocity. With initial concentration increased from 0.25 to 0.79 ppm at face velocity 0.25 to and 0.75 m s^{-1}, the rate constant (k_2) values were increased from 0.323, 0.4, and 0.409 to 0.715, 0.716, and 0.721 g mg^{-1} min^{-1}, respectively. Moreover, the calculated $q_{e,2}$ values are closer to the experimental data, the rate constant (k_2) of the pseudo-second-order rate model related to formaldehyde initial concentration (C_0) is shown in Fig. 15. This result is similar to the findings of many previous studies (Saeid and Bahare, 2006).

Intraparticle Diffusion Model

Fig. 16 shows the plot of intraparticle diffusion model. The rate constants (k_i) are obtained from the slope of the

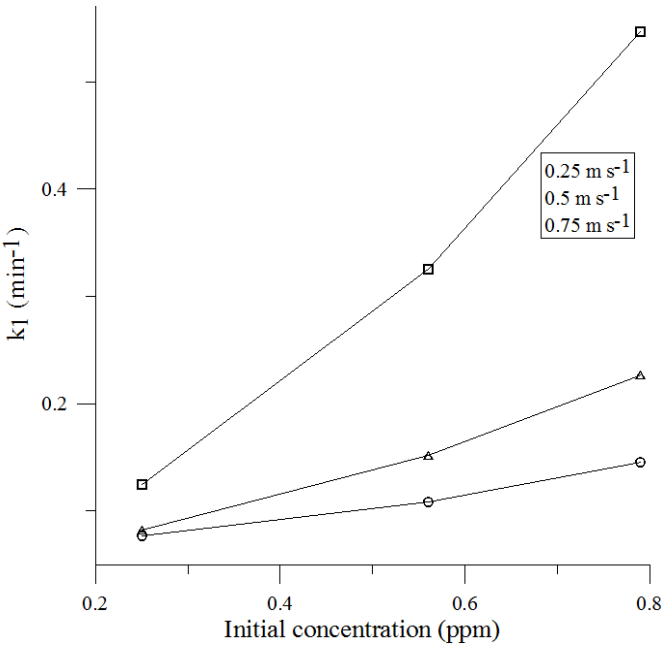

Fig. 13. The relationship between the Pseudo-first-order rate constant and formaldehyde initial concentration.

line on second stage. C value of the intercept demonstrated some degree boundary layer thickness. It is larger to promote the greater effect of the boundary layer. k_i and C value with its correlation coefficients are shown in Table 5. The adsorption process presented three steps: Stage 1: The adsorbate molecules are diffused in the adsorption and adsorbed on the outer surface (Shiue and Hu, 2012; Tang *et al.*, 2016; Hu *et al.*, 2017; Shiue *et al.*, 2017). Stage 1 is finished before 2 min average at 0.25 to 0.79 ppm inlet formaldehyde concentrations of 0.25, 0.5, and 0.75 m s^{-1} face velocity, respectively. Stage 2: this stage is a developed process and k_i is the highest, resulting that the intraparticle diffusion is the key controlling factor of adsorption rate (Shiue and Hu, 2012; Tang *et al.*, 2016; Hu *et al.*, 2017; Shiue *et al.*, 2017). It kept and continues from 2 min to 25–49, 16–36, and 9–25 min of AC adsorptive filter media at 0.25 to 0.79 ppm inlet concentration of 0.25, 0.5, and 0.75 m s^{-1} face velocities, respectively. Stage 3: This stage is the adsorption equilibrium process, where the intraparticle diffusion further slows down, and the adsorption rate

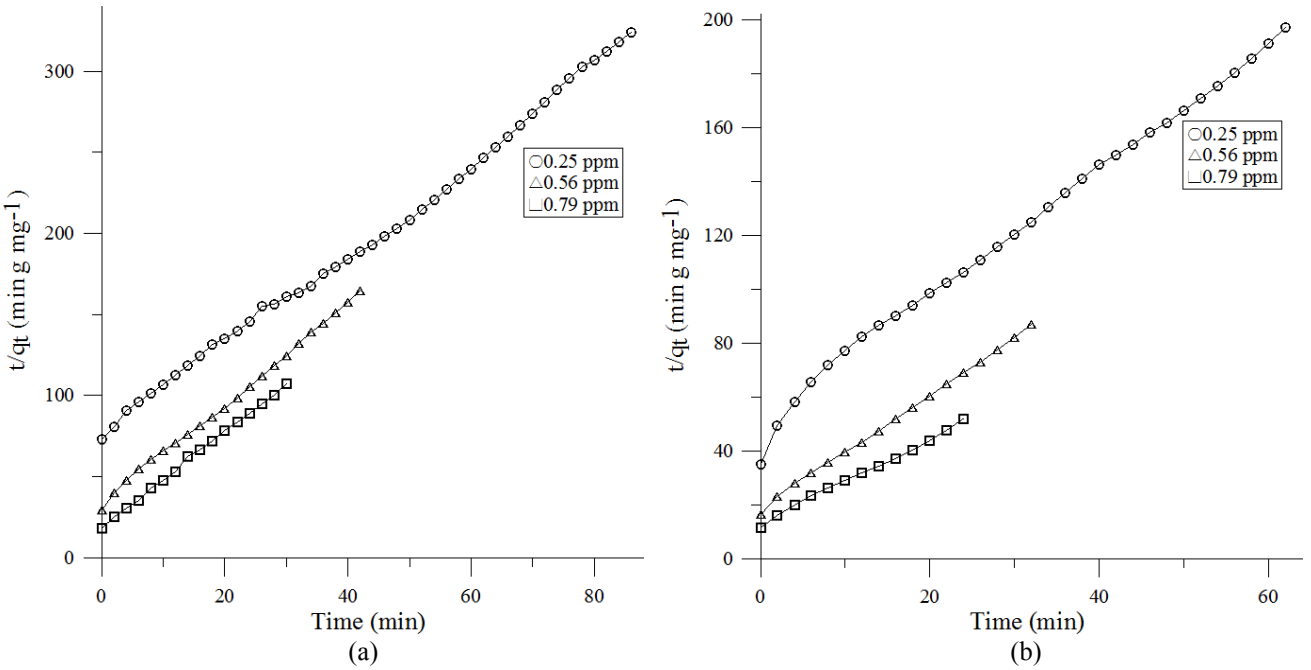

Fig. 14. Plot of Pseudo-second order kinetic for the adsorption of formaldehyde at face velocity (a) 0.25 m s^{-1}, (b) 0.5 m s^{-1}, and (c) 0.75 m s^{-1}.

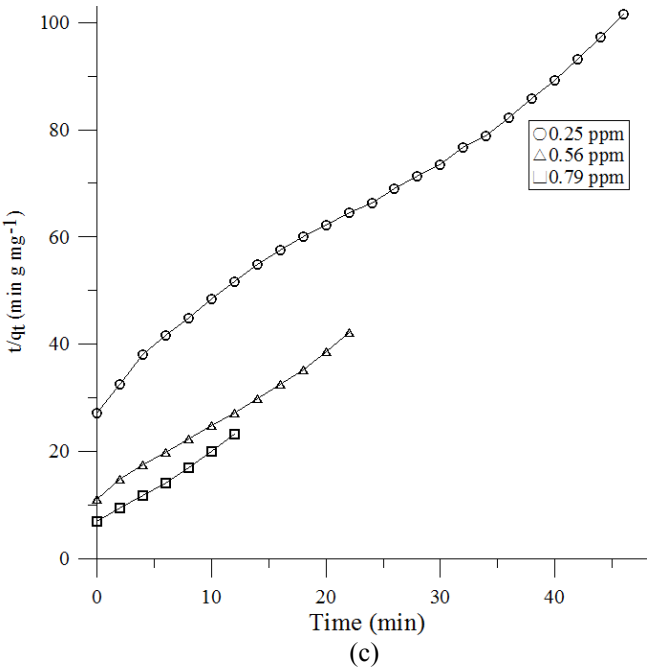

Fig. 14. (*continued*).

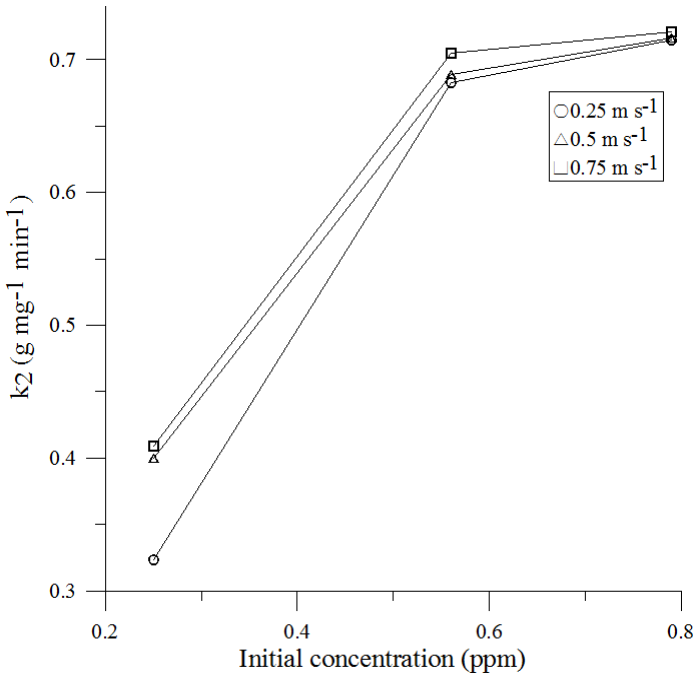

Fig. 15. The relationship between the Pseudo-second-order rate constant and formaldehyde initial concentration.

decreases significantly due to the adsorbates almost filled the micropores and mesopores (Shiue and Hu, 2012; Tang *et al.*, 2016; Hu *et al.*, 2017; Shiue *et al.*, 2017). It starts after the above mentioned time schedule at 0.25 to 0.79 ppm inlet formaldehyde concentration of 0.25, 0.5, and 0.75 m s^{-1} face velocity, respectively. The formaldehyde is slowly removed via intraparticle diffusion into the particles and is finally kept in the micropores. Generally, intraparticle diffusion rate constant k_i is the slope of the Stage 2 line. The values of k_i arise from 0.031 to 0.049 $min^{-1/2}$ (0.25 m s^{-1}), from 0.041 to 0.089 $min^{-1/2}$ (0.5 m s^{-1}), and from 0.072 to 0.133 $min^{-1/2}$ (0.75 m s^{-1}) of AC adsorptive filter media when increase from 0.25 ppm to 0.79 ppm, respectively. Nevertheless, the linear intercept C is not zero and larger, showing that the membrane diffusion in Stage 3 also affected the adsorption rate (Tang *et al.*, 2016). Three stage of the intraparticle diffusion model fitted the adsorption data well. The formaldehyde adsorption onto AC adsorptive filter media is affected by combined intraparticle diffusion model and membrane diffusion (Tang *et al.*, 2016).

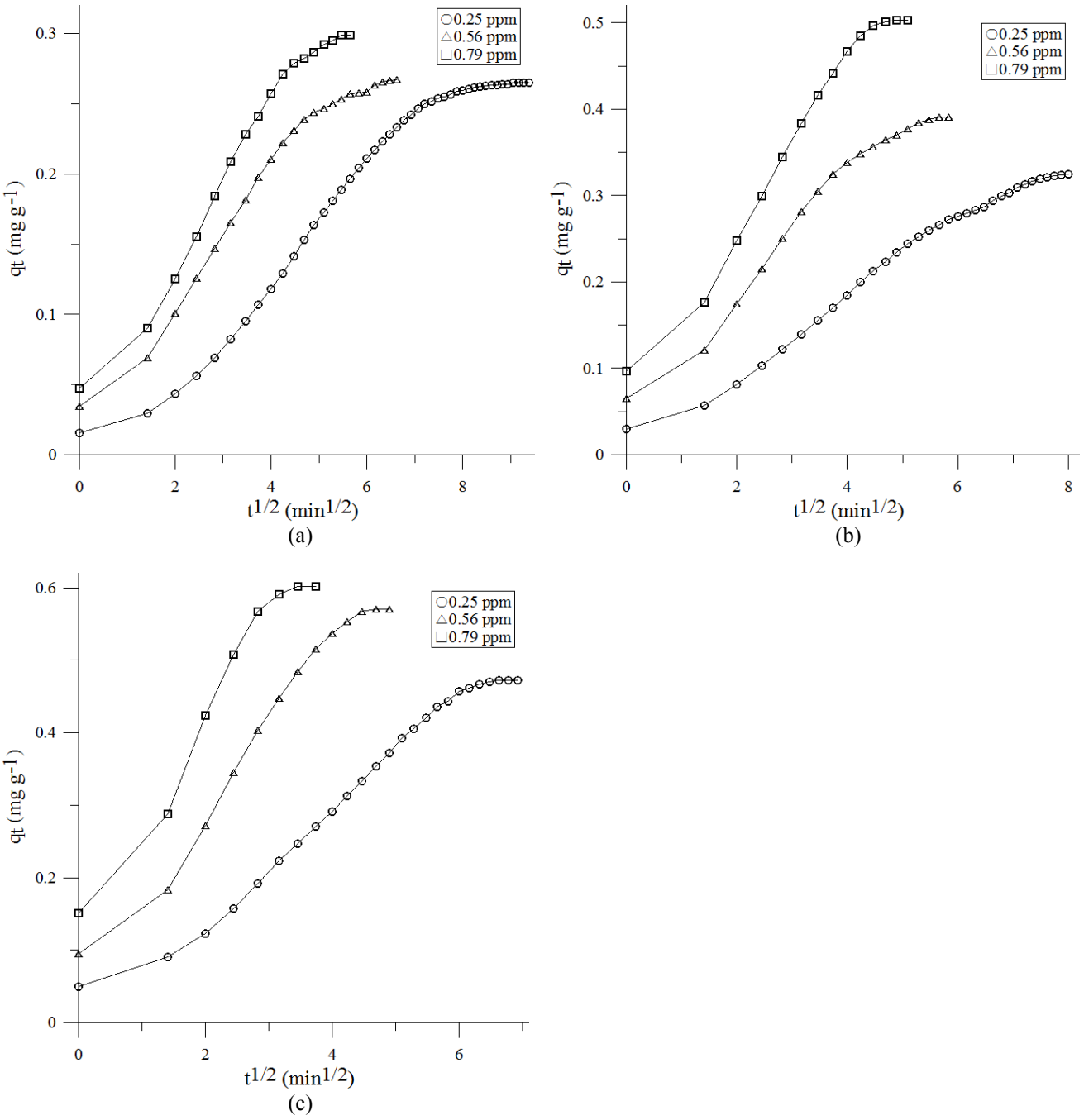

Fig. 16. Plot of intraparticle diffusion model at face velocity (a) 0.25 m s^{-1}, (b) 0.5 m s^{-1}, and (c) 0.75 m s^{-1}.

Error Analysis

The correlation coefficients of the pseudo-second-order kinetic model (average value = 0.969) is higher than the pseudo-first-order kinetic model (average value = 0.899) and the intraparticle diffusion model (average value = 0.863). This result is similar to the findings by Tsai *et al.* (2017) and Adelodun *et al.* (2016). For the adsorption process, physisorption might be the controlling mechanism by the highest correlation coefficient (average value = 0.969) and the lowest mean absolute percentage error value (average MAPE < 8%) verification. Only the intraparticle diffusion model fits the experimental data. Thus, it was determined to be the rate limiting step for the initial period of the adsorption process.

Adsorption Isotherms

The plots of the Freundlich and Langmuir isotherm models are presented as Figs. 17 and 18, respectively. The isotherm constants and maximum adsorption capacity (q_{max}) values are listed in Table 6. According to the linear regression method, the formaldehyde adsorption by AC adsorptive filter media exhibits a better fit to Langmuir equation was statistically confirmed by giving greater R^2 values closer to unity (R^2 > 0.987). This denotes that the Langmuir model

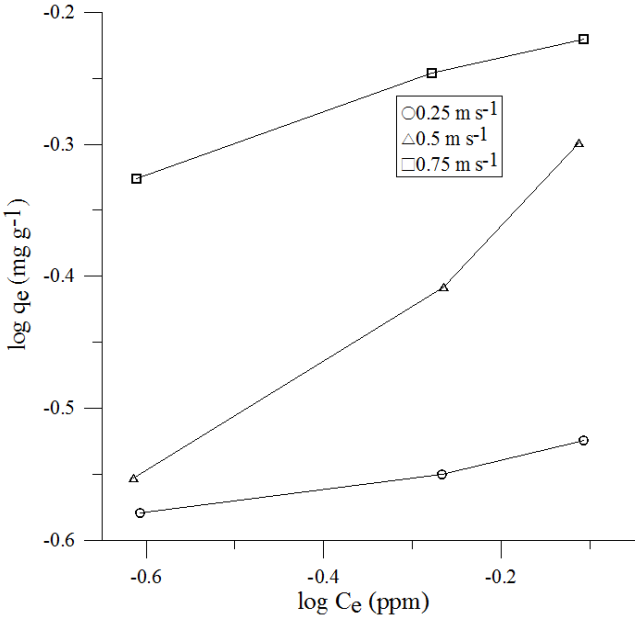

Fig. 17. Formaldehyde adsorption with Freundlich adsorption isotherm.

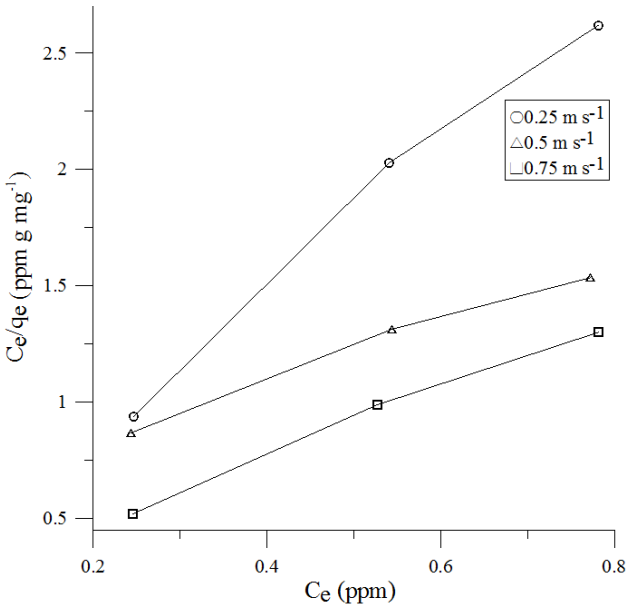

Fig. 18. Formaldehyde adsorption with Langmuir adsorption isotherm.

may better describe an adsorption isotherm for AC adsorptive filter media. This adsorptive behavior pointed out that the adsorption occurs on a heterogeneous surface, which may be aspect to the various active sites on AC adsorptive filter media. The overall adsorptive performance prevails as a physical adsorption process. This phenomenon has been described before (Cheng and Tsai, 2007; Bernabe *et al.*, 2015). The results show that the maximum formaldehyde adsorption capacity (q_{max}) of AC adsorptive filter media was 0.7862 mg g^{-1} at 0.75 m s^{-1} face velocity. From the observed results we conclude that AC adsorptive filter media is potentially a good solution for formaldehyde removal.

Table 5. Fitting parameters of three kinetic models for formaldehyde adsorption.

Face velocity	Inlet concentration	Pseudo-first-order			Pseudo-second order			Intraparticle diffusion			
		k_1 (min^{-1})	$q_{e,1}$ (mg g^{-1})	r_1^2	MAPE (%)	k_2 (g mg^{-1} min^{-1})	$q_{e,2}$ (mg g^{-1})	r_2^2	MAPE (%)	Ki (mg g^{-1} $min^{-1/2}$)	C	r_i^2	MAPE (%)
0.25 m s^{-1}	0.25 ppm	0.077	0.571	0.915	161.51	0.323	0.309	0.96	5.49	0.031	0.019	0.846	12.43
	0.56 ppm	0.108	0.349	0.969	14.96	0.683	0.329	0.984	2.35	0.037	0.053	0.813	7.89
	0.79 ppm	0.145	0.291	0.977	25.27	0.715	0.35	0.973	4.63	0.049	0.057	0.867	6.4
0.5 s^{-1}	0.25 ppm	0.082	0.787	0.803	88.69	0.4	0.402	0.972	3.92	0.041	0.048	0.895	6.69
	0.56 ppm	0.142	0.548	0.959	20.69	0.689	0.436	0.983	3.67	0.06	0.087	0.832	6.57
	0.79 ppm	0.227	0.441	0.896	119.21	0.716	0.522	0.972	5.46	0.089	0.11	0.871	5.67
0.75 m s^{-1}	0.25 ppm	0.125	0.986	0.795	156.27	0.409	0.498	0.94	5.94	0.072	0.055	0.924	8.72
	0.56 ppm	0.225	0.825	0.896	64.36	0.705	0.785	0.965	6.12	0.109	0.103	0.876	7.06
	0.79 ppm	0.547	0.82	0.878	66.19	0.721	0.919	0.974	7.92	0.133	0.153	0.843	5.93

Table 6. Freundlich and Langmuir isotherm parameters.

Face velocity	Freundlich isotherm			Langmuir isotherm		
(m s^{-1})	K_f (mg g^{-1})(L $mg^{-1})^{1/n}$	1/n	R^2	q_{max}(mg g^{-1})	K_L (L mg^{-1})	R^2
0.25	0.5965	0.1061	0.9738	0.3167	15.2046	0.9872
0.5	0.6121	0.2133	0.9794	0.6864	8.058	0.9879
0.75	0.8242	0.4908	0.9886	0.7862	2.2	0.9923

Except than the Freundlich and Langmuir isotherms, the experimental data were also represented by the D-R equation. Fig. 19 was plotted as lnW versus A^2 for AC filter from adsorption isotherms of N_2 data of Fig. 3. As shown in the figure, the characteristic curve for formaldehyde is simulated linearly at a lower A^2 range. Nevertheless, the isotherm data of formaldehyde cannot be linearly fitted over the entire range of abscissa. A clear transition was observed at ~2.2×10^7 J^2 mol^{-2} of A^2, which is equal to a relative pressure (P/Po) of 0.151 for the adsorbates to represent a good fit at lower levels of A^2 (high P/Po) and of a big discrepancy at high A^2 (low P/Po) in agreement with Shiue *et al.* (2011) research work. The results show that the D-R equation can simulate the experimental adsorption data except very low relative pressures. In the event of relative pressures lower than 0.151, the D-R equation may be difficult to utilize the simulation of the adsorption capacity for the tested adsorption systems.

CONCLUSIONS

According to this study, formaldehyde removal by AC adsorptive filter media is effective in indoor environments. The SEM images showed that AC surface were rather uneven, with coarse and small pores. Irregular layer structures were formed amorphously, and the XRD diffraction peaks were broad. C, O, Mg, P etc. were detected via EDS analysis, which showed that the Mg/C ratio = 0.68% and further proves the existence of MgO in AC. According to BET analysis checked with FTIR, the surface area was 1333.3304 m^2 g^{-1}, and ketone -C=O bonds, which explain the presence of a sensible peak at 3417 cm^{-1} and weak strength bonding at 2329 cm^{-1}, were successfully grafted onto the carbon.

The results indicate that an increased initial concentration of formaldehyde and face velocity is associated with a higher adsorption capacity and faster breakthrough time. The breakthrough behavior at low formaldehyde concentrations can be linearly expressed by the relationship between the natural logarithm of the breakthrough time and the natural logarithm of the initial concentration. High correlation coefficients ($R^2 > 0.972$) for the formaldehyde adsorption onto the coconut activated carbon filter media confirm good agreement between the Yoon-Nelson model and the experimental data. Regarding the adsorption kinetics of formaldehyde removal by AC adsorptive filter media, the pseudo-second-order model displayed the highest correlation coefficient ($0.94 < R^2 < 0.984$) and lowest MAPE values

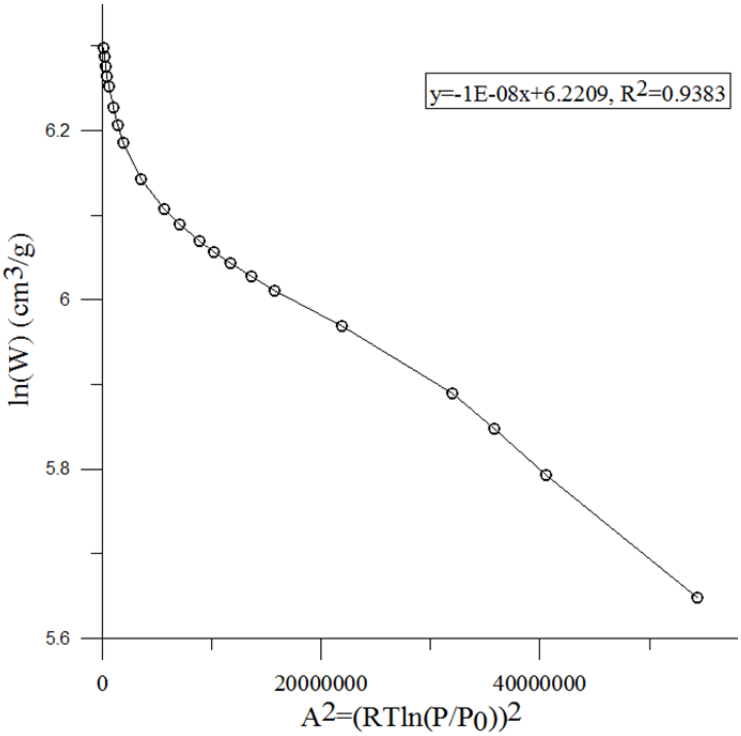

Fig. 19. The D-R isotherm.

(8%), demonstrating more accurate prediction than the pseudo-first-order model; the intraparticle diffusion model and membrane diffusion was able to predict the adsorption kinetics. The Langmuir equation is well-fitted to the AC adsorptive filter. The D-R equation successfully predicted the equilibrium capacity of AC to adsorb formaldehyde at high relative pressures. Overestimation of the adsorption capacity was detected when predicting the formaldehyde adsorption capacity at relative pressures below 0.151.

ACKNOWLEDGEMENTS

The authors would like to acknowledge the supports from the Ministry of Science and Technology with contract number 105-3011-F-027-001.

NOMENCLATURE

C intercept of intraparticle diffusion model, mg kg^{-1}
Ce concentration of free formaldehyde in air, ppm
C_0 the inlet concentration, ppm
k_1 the pseudo-first-order rate coefficient, min^{-1}
k_2 the pseudo-second-order rate coefficient, g mg^{-1} min^{-1}
k_i the intraparticle diffusion rate constant, mg g^{-1} min$^{-1/2}$
K_L the Langmuir's adsorption equilibrium constant related to the affinity of the binding sites, L mg^{-1}
q_e the amount of adsorbed formaldehyde per unit weight of adsorbent, mg g^{-1}
q_{max} maximum adsorption capacity, mg g^{-1}
q_t the amount of adsorbate adsorbed at time t, mg g^{-1}
t testing time, min
V the airflow rate, L min^{-1}

REFERENCES

Adelodun, A.A., Ngila, J.C., Kim, D.G. and Jo, Y.M. (2016). Isotherm, thermodynamic and kinetic studies of selective CO_2 adsorption on chemically modified carbon surfaces. *Aerosol Air Qual. Res.* 16: 3312–3329.

Bernabe, D.P., Herrera, R.A.S., Doma Jr, B.T., Fu, M.L., Dong, Y. and Wang, Y.F. (2015). Adsorption of low concentration formaldehyde in air using ethylene-diamine modified diatomaceous earth. *Aerosol Air Qual. Res.* 15: 1652–1661.

Boehm, H.P. (2002). Surface oxides on carbon and their analysis: A critical assessment. *Carbon* 40: 145–149.

Bolis, V. (2013). Fundamentals in adsorption at the solid-gas interface. Concepts and thermodynamics, In *Calorimetry and thermal methods in catalysis*, Auroux, A. (Ed.), Springer Berlin Heidelberg, Berlin, Heidelberg, pp. 3–50.

Brunsgaard, C., Heiselberg, P., Knudstrup, M.A. and Larsen, T.S. (2012). Evaluation of the indoor environment of comfort houses: Qualitative and quantitative approaches. *Indoor Built Environ.* 21: 432–451.

Cheng, W.H. and Tsai, S.C. (2007). Competition among mixed adsorbates affecting the adsorption of gaseous methyl ethyl ketone by hydrophobic molecular sieve. *Aerosol Air Qual. Res.* 7: 205–220.

Cheng, W.H. (2008). Adsorption Characteristics of granular activated carbon and SPME indication of VOCs breakthrough. *Aerosol Air Qual. Res.* 8: 178–187.

Chuck, W.F. and Kim, J.T. (2013). Photocatalytic oxidation for maintenance of indoor environmental quality. *Indoor Built Environ.* 22: 39–51.

Carpiné, D., Dagostin, J.L.A., da Silva, V.R., Igarashi-Mafra, L. and Mafra, M.R. (2013). Adsorption of volatile aroma compound 2-phenylethanol from synthetic solution onto granular activated carbon in batch and continuous modes. *J. Food Eng.* 117: 370–377.

Dehdashti, A., Khavanin, A., Rezaee, A., Assilian, H. and Motalebi, M. (2011). Application of microwave irradiation for the treatment of adsorbed volatile organic compounds on granular activated carbon. *Iran. J. Environ. Health Sci. Eng*. 8: 85–94.

Dubinin, M.M. (1966). Porous structure and adsorption properties of active carbons. In Chemistry and physics of carbon, Vol. 2, Walker, P.L. (Ed.), Marcel Dekker, New York, pp. 51–120.

Gilbert, N.L., Guay, M., Gauvin, D., Dietz, R.N., Chan, C.C. and Lévesque, B. (2008). Air change rate and concentration of formaldehyde in residential indoor air. *Atmos. Environ.* 42: 2424–2428.

Guibal, E. (1998). Metal-anion sorption by chitosan beads: Equilibrium and kinetic studies. *Ind. Eng. Chem. R*es. 37: 1454–1463.

Ho, Y.S. and McKay, G. (1998). The kinetics of sorption of basic dyes from aqueous solution by sphagnum moss peat. C*an. J. Chem. Eng.* 76: 822–827.

Jo, W.K. and Chun, H.H. (2014). Application of fibrous activated carbon filter in continuous-flow unit for removal of volatile organic compounds under simulated indoor conditions. *Aerosol Air Qual. Res.* 14: 347–354.

Lagergren, S. (1898). Zur theorie der sogenannten adsorption geloster stoffe, Kungliga Svenska Vetenskapsakademiens. *Handling* 24: 1–39.

Liang, W., Li, J. and Jin, Y. (2012). Photo-catalytic degradation of gaseous formaldehyde by TiO_2/UV, Ag/TiO_2/UV and Ce/TiO_2/UV. *Build. Environ.* 51: 345–350.

Lu, C.L., Pan, L.W. and Zhu, B. (2015). Study the Static adsorption-desorption of formaldehyde on activated carbons. International Forum on Energy, Environment Science and Materials (IFEESM), pp. 943–947.

Lu, N., Pei, J.J., Zhao, Y.X., Qi, R.Y. and Liu, J.J. (2012). Performance of a biological degradation method for indoor formaldehyde removal. *Build. Environ.* 57: 253–258.

Malina, J.A. and Rađenović, A. (2014). Kinetic aspects of methylene blue adsorption on blast furnace sludge. *Chem. Biochem. Eng. Q*. 28: 491–498.

Mandal, S., Mahapatra, S.S., Adhikari, S. and Patel, R.K. (2015). Modeling of arsenic (III) removal by evolutionary genetic programming and least square support vector machine models. *Environ. Processes* 2: 145–172

Mui, K.W., Wong, L.T. and Hui, P.S. (2008). Policy influence of formaldehyde exposure risk in air-conditioned office environment. *Indoor Built Environ.* 17: 449–454.

Rengga, W.D.P., Sudibandriyo, M., Mohammad Nasikin, M. (2016). Adsorptive removal of formaldehyde by chemically bamboo activated carbon with addition of Ag nanoparticle: Equilibrium and Kinetic. *MATEC Web of Conferences* 5: 04004.

Saeid, A. and Bahare, Y. (2006). Adsorption of 18-crown-6 from aqueous solution on granular activated carbon: A kinetic modeling study. *J. Colloid Interface Sci.* 299: 112–115.

Scahill, J., Wolfrum, E.J., Michener, W.E., Bergmann, M., Blake, D.M. and Watt, A.S. (2004). A new method for the rapid determination of volatile organic compound breakthrough times for a sorbent at concentrations relevant to indoor air quality. *J. Air Waste Manage. Assoc.* 54: 105–110.

Shiue, A., Kang, Y.H., Hu, S.C., Jou, G.T., Lin, C.H., Hu, M.C. and Lin, S.I. (2010). Vapor adsorption characteristics of toluene in an activated carbon adsorbent-loaded nonwoven fabric media for chemical filters applied to cleanrooms. *Build. Environ.* 45: 2123–2131.

Shiue, A., Den, W., Kang, Y.H., Hu, S.C., Jou, G.T., Lin, C.H., Hu, V. and Lin, S.I. (2011). Validation and application of adsorption breakthrough models for the chemical filters used in the make-up air unit (MAU) of a cleanroom. *Build. Environ.* 46: 468–477.

Shiue, A. and Hu, S.C. (2012). Adsorption kinetics for the chemical filters used in the make-up air unit (MAU) of a cleanroom. *Sep. Sci. Technol.* 47: 577–583.

Tsai, C.Y., Chiu, C.H., Chuang, M.W. and His, H.C. (2017). Influences of copper(II) chloride impregnation on activated carbon for low-concentration elemental mercury adsorption from simulated coal combustion flue gas. *Aerosol Air Qual. Res.* 17: 1637–1648.

U.S. Consumer Product Safety Commission (2015). An updated on formaldehyde. U.S. Consumer Product Safety Commission, USA.

VanOsdell D.W., Owen M.K., Jaffe L.B. and Sparks L.E. (1996). VOC removal at low contaminant concentrations using granular activated carbon. *J. Air Waste Manage. Assoc.* 46: 883–890.

Vimonses, V., Lei, S., Jin, B., Chow, C.W.K. and Saint, C. (2009). Kinetic study and equilibrium isotherm analysis of Congo Red adsorption by clay materials. *Chem. Eng. J.* 148: 354–364.

Wang, Z.Q., Pei, J.J., Jensen, S. and Zhang, J.S. (2014). Experimental investigation of the formaldehyde removal mechanisms in a dynamic botanical filtration system for indoor air purification. *J. Hazard. Mater.* 280: 235–243.

Yao, M., Zheng, Q., Hand, D.W. and Perram, L. (2009). Investigation of the treatability of the primary indoor volatile organic compounds on activated carbon fiber cloths at typical indoor concentrations. *J. Air Waste Manage. Assoc.* 59: 882–890.

Ye, J.J., Ye, F., Dai, W. and Ding, D. (2015). Formaldehyde capture with finger citron residue based activated carbon. *Sep. Sci. Technol.* 50: 253–259.

Yu, C.W.F. and Kim, J.T. (2010). Building pathology, investigation of sick buildings – VOC emissions. *Indoor Built Environ.* 19: 30–39.

Received for review, April 9, 2018
Revised, July 12, 2018
Accepted, July 16, 2018